Euro. Jnl of Applied Mathematics (2021), *vol.* 32, *pp.* 806–819
doi:10.1017/S0956792520000418

A proposed screening algorithm for bone remodelling

C. F. ARIAS[1], F. BERTOCCHINI[1], M. A. HERRERO[2], J. M. LÓPEZ[3] and G. E. OLEAGA[2]

[1]*Centro de Investigaciones Biológicas, CSIC, Ramiro de Maeztu 9, 28040 Madrid, Spain*
[2]*Departamento de Análisis Matemático y Matemática Aplicada, Facultad de Matemáticas, Universidad Complutense, 28040 Madrid, Spain*
email: goleaga@ucm.es
[3]*Departamento de Morfología y Biología Celular, Universidad de Oviedo, 33006 Oviedo, Asturias, Spain*

(*Received 25 May 2020*; *revised 19 October 2020*; *accepted 27 November 2020*; *first published online 23 December 2020*)

One of the most remarkable aspects of human homoeostasis is bone remodelling. This term denotes the continuous renewal of bone that takes place at a microscopic scale and ensures that our skeleton preserves its full mechanical compliance during our lives. We propose here that a renewal process of this type can be represented at an algorithmic level as the interplay of two different but related mechanisms. The first of them is a preliminary screening process, by means of which the whole skeleton is thoroughly and continuously explored. This is followed by a renovation process, whereby regions previously marked for renewal are first destroyed and then rebuilt, in such a way that global mechanical compliance is never compromised. In this work, we pay attention to the first of these two stages. In particular, we show that an efficient screening mechanism may arise out of simple local rules, which at the biological level are inspired by the possibility that individual bone cells compute signals from their nearest local neighbours. This is shown to be enough to put in place a process which thoroughly explores the region where such mechanism operates.

Key words: Mathematical modelling and simulation, bone remodelling, biological algorithms, cellular automata, osteocytes

2020 Mathematics Subject Classification: (Primary) 92-08 Computational methods for problems pertaining to biology; 92-10 Mathematical modelling or simulation for problems pertaining to biology. (Secondary) 92C30 Physiology (general); 92C42 Systems biology, networks; 92B25 Biological rhythms and synchronisation.

1 Introduction

The human skeleton is composed of over 200 bones of different shapes and sizes. Altogether they make up for a complex organ that performs essential functions in ordinary life. To begin with, it provides a physical frame to protect internal body organs. In addition, it transmits the force arising from muscle contraction required for movement and provides a reservoir for minerals, particularly calcium.

In the course of our daily activities, bones are subject to a homoeostatic renewal process that ensures microdamage repair and maintains their structural integrity. In fact, to remain operative,

our bones undergo continuous renovation through repeated cycles of demolition and rebuilding. By means of this process, termed as bone remodelling, every single bone is eventually screened out for mechanical compliance, with the result that old bone is systematically replaced by freshly made one. Bone remodelling is known to occur anytime and anywhere in the body. At any single moment, bone is simultaneously resorbed at millions of sites throughout the body and is replaced shortly afterwards in a distributed, microscopic manner, so that the bulk of the skeleton always remains fully operational [4, 17] and its total volume and weight are kept basically constant. In adults, around 10% of the skeleton is estimated to be involved in bone remodelling at any time, so that the whole skeleton is renewed approximately every 10 years [1]. This dynamic activity is crucial to preserve a healthy skeleton. Any dysfunction of this continuous maintenance activity would eventually lead to generalised mechanical failure with fatal consequences.

Bone remodelling is known to be a tightly regulated, multicellular process involving different cell types. Key agents are osteocytes, osteoblasts and osteoclasts, each performing different but coordinated tasks. In short, bone remodelling can be summarised as follows. As a consequence of a mechanism that remains only partially known, a particular region of bone, which could be thought of as a mineral matrix interspersed with osteocytes (the basic bone cell type), is at some time marked for remodelling. This means that such region will first be destroyed by a specialised cell type (osteoclasts) after which new bone will be yield by another cell type (osteoblasts) in the empty space thus left. Osteoclasts and osteoblasts are derived from different progenitor pools located at the bone marrow and organise together to form a committed team of cells known as basic multicellular units (BMUs) which involves a few hundred cells and move inwards into the bone over regions a few hundred microns in diameter. Active BMUs consist of a head portion or leading front of bone resorbing osteoclasts and a tail portion of bone-synthetising osteoblasts moving in the wake of the former. BMUs are recruited for remodelling where and when needed and cease to exist once their task has been accomplished. In particular, as renewal of the selected zone nears completion, all the osteoclasts and most osteoblasts disappear. A few remaining osteoblasts become surrounded by the bone matrix they secrete and differentiate into osteocytes. When such differentiation is completed, a piece of new bone has been formed in place of the former one. In due time, such new bone will be disposed of by means of the same process which we have just sketched [14, 15, 23, 32].

Mature osteocytes are thus individually encased inside spaces of the mineralised matrix called lacunae, but they form dendritic cytoplasmic processes that extend out from their lacunae into minute ducts named canaliculi, which in turn connect different lacunae. Osteocytes are thus connected with their neighbours via these dendritic processes and form an extensive cellular network throughout the entire skeleton (see Figure 1). This connecting network is thought to play a prominent role in the detection of mechanical and hormonal stimuli, eventually resulting in bone remodelling at appropriate sites of the skeleton [5].

While much progress has been achieved in identifying the molecular signals involved in the regulation of osteoclast and osteoblast differentiation and activity [8, 14, 31, 32] the mechanisms associated with bone remodelling in general, and with BMUs activation in particular, remain largely unknown. In particular, remodelling is thought to be elicited to repair microfractures [26, 28], and we have recently proposed a possible cell algorithm to account for BMU operation in such situation [2]. Remodelling in response to microfractures involves a wide range of control mechanisms that include both internal and external factors. Many systemic hormones as well as local factors are essential for the proper coupling of bone formation and

https://doi.org/10.1017/S0956792520000418 Published online by Cambridge University Press

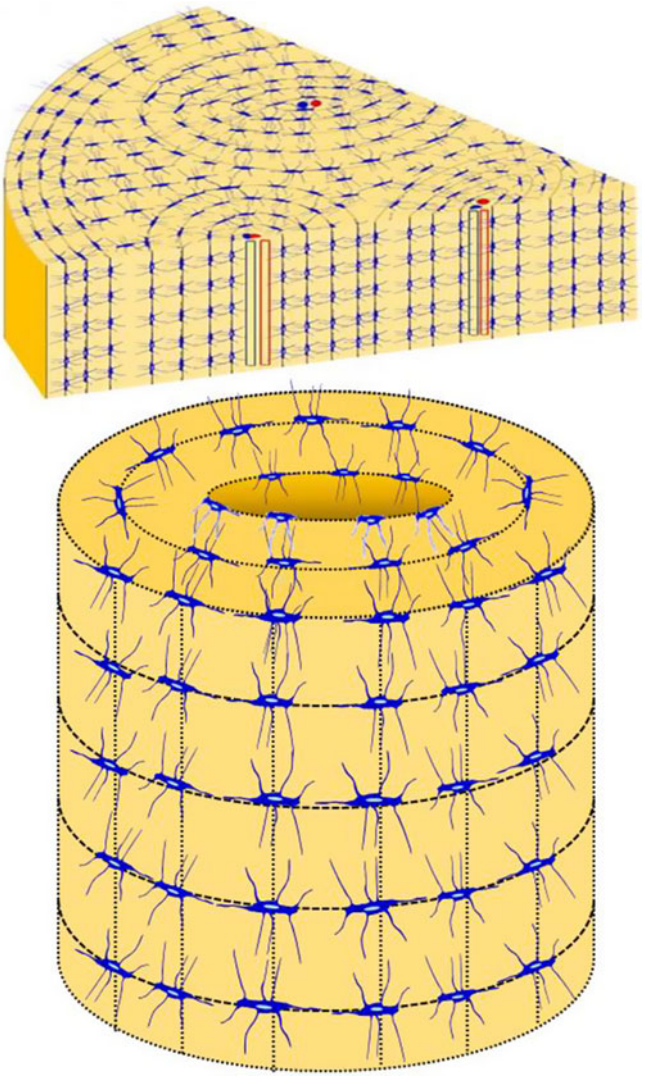

FIGURE 1. Microscopical structure of cortical bone of the shaft of a long bone.

Top: Scheme of the compact bone with most of the osseous tissue arranged in compact cylinders of concentric lamellae (osteons) around a central canal (Haversian canal) containing blood vessels.

Below: Scheme of an osteon as a compact cylinder of concentric bone matrix layers with the osteocytes sandwiched between adjacent lamellae. Osteocytes are regularly arranged throughout the mineralised matrix in cavities called lacunae and connected to each other through thin cytoplasmic branching processes called canaliculi. The canaliculi provide an extensive intracellular and extracellular communication system between osteocytes.

bone resorption [30, 31]. However, it is becoming increasingly clear that these hormonal and paracrine signals are linked with mechanical and environmental stimuli [16, 24, 25]. A number of studies have explored the use of mathematical models, both of a local and non-local nature, to achieve quantitative and qualitative insight into molecular and mechanical pathways regulating bone function [7, 9, 11–13, 16, 19–21, 24, 25, 27, 29–31]. Here, we follow this approach to address

https://doi.org/10.1017/S0956792520000418 Published online by Cambridge University Press

a question that remains unanswered, namely how can bone remodelling be kept continuously operative, so that the whole skeleton be periodically renewed. We suggest that bone remodelling should not be limited to an on–off repair system activated after local bone injuries. It seems unlikely that such process should be a mere reaction to local damage, and that the latter could be so widespread as to ensure continuous, and exhaustive, remodelling throughout a lifetime. We propose instead that a detection mechanism should be continuously operating all over the skeleton and is instrumental in marking those bone regions that must be remodelled even if no damage (as that arising from microfractures) has yet occurred there. Providing a possible algorithmic candidate for such screening process, the basic backstage upon which bone remodelling will eventually unfold is the goal of this article.

Specifically, the question we want to address here can be formulated as follows. We want to describe a possible bone – screening algorithm that fulfills the following criteria:

(i) Provides continuous surveillance,
(ii) Allows every single bone region to be eventually explored,
(iii) Can be switched on or off externally if necessary (for instance, in case of microfracture) but routinely works in absence of such stimuli.
Moreover, while ascertaining the precise biological processes behind this hypothetical mechanism is beyond the scope of this work, care will be taken to ensure that:
(iv) The operational rules of the proposed screening mechanism are compatible with current knowledge of bone cell biology.

Concerning this last issue, we use as a starting point a picture of the skeleton as a medium where a number of agents (osteocytes) are distributed to form a regularly spaced, intercommunicated network. Osteocytes are known to produce a molecular signal (sclerostin) that inhibits osteoblasts differentiation from their mesenchymal precursors [8, 22] thus preventing BMU activation. It is also well known that only when the local concentration of sclerostin falls below some threshold value, osteoblasts cease can be inhibited, which allows the process of bone remodelling to begin. Remarkably, concerning sclerostin, osteocytes seem to be in one of two discrete states: expressing or not expressing it (see Figure 2). This suggests an interesting analogy with neurons, which can also be found in electrically active and inactive states concerning the transmission of nerve impulses.

Based on these observations, we suggest that osteocytes routinely carry out a decision algorithm that results in the propagation of activation and deactivation patterns across the osteocyte network in bone. In particular, the main assumption of the model provided below is that the state of each cell depends on the states of neighbouring cells. At the mathematical level, we propose that such a decision mechanism can be described by means of a Cellular Automaton model [6, 18] subject to quite simple decision rules. In fact, the corresponding algorithm is endowed with transition rules inspired by the classical Conway's 'Game of Life' [10] as described in our next section.

We will show that such simple computing rules suffice to guarantee that alternating patterns of activation and deactivation eventually visit every single place at a bone surface, thus providing an efficient screening mechanism over that surface. This is a preliminary step towards ensuring that in due time, inward-bound BMUs will be periodically generated all over the whole bone boundary. The question of coupling a screening algorithm with others(s) that first trigger and then rule BMU operation (for which a possible candidate has been suggested in [2]) remains

https://doi.org/10.1017/S0956792520000418 Published online by Cambridge University Press

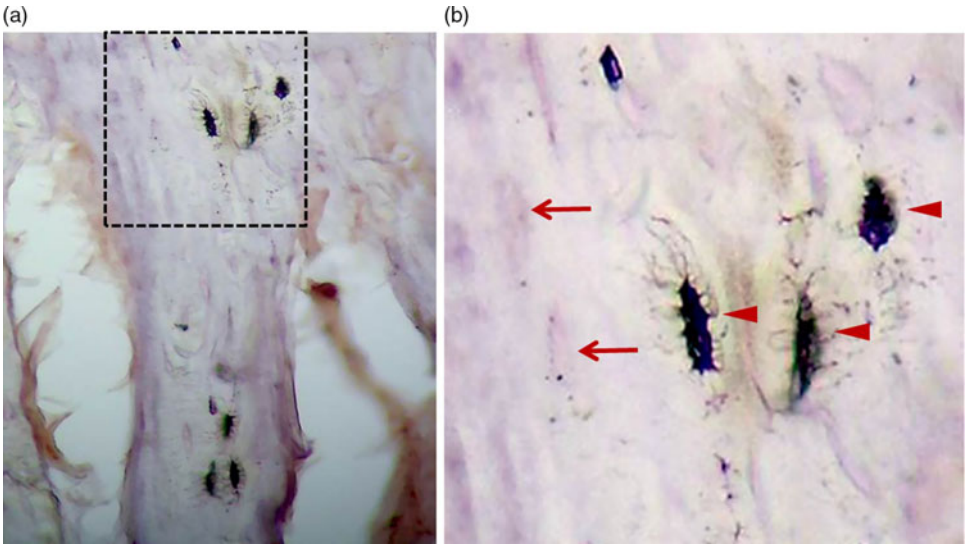

FIGURE 2. Immunohistochemical localisation of sclerostin in a longitudinal section from a rat tibia. The photomicrograph (a) shows the presence in secondary trabeculae of some osteocytes with intense reactivity (brown colour), while other osteocytes are negative for sclerostin staining. The inset is enlarged in (b) and shows that positive osteocytes (arrowheads) show intense signal in both the perinuclear cytoplasm and osteocyte canaliculi and/or cell processes. Arrows show osteocytes with no detectable sclerostin expression.

open at this stage, as does the quantitative regulation of operational space and timescales in our model so that they remain within observed biological parameters. We intend to address some of these questions in future work.

2 The proposed screening algorithm

We consider in this section a two-dimensional domain in the shape of a chessboard B consisting of N by N smaller squares, b_{ij}, each being occupied by a bone cell. This domain will then be folded to produce a cylinder, and we will focus our attention in one (arbitrarily chosen) of the generatrix lines along the resulting cylinder. Each of the smaller squares having one side over such line will be assumed to be in one of two states that will be termed as active and inactive, respectively. While the underlying conditions which determine active and inactive states may be quite complex, it may be useful to associate active and inactive states with the expression and inhibition of sclerostin, respectively. An initial distribution of active and inactive cells is selected randomly (See Figure 3). For instance, any square in the chessboard is labelled as active with probability p $(0 < p < 1)$ or inactive with probability $1 - p$. Once the initial configuration is fixed, we let it evolve according to the following rules:

(a) For any given interior square b_{ij}, we define its neighbours as the set of squares b_{nm} such that $0 < |i - n| \leq 2$, $0 < |j - m| \leq 2$. In order to satisfy homogeneous Dirichlet conditions at the lateral sides of the domain and to ensure consistency of the simulations, we assume some auxiliary (and artificial) boundary conditions as follows. In particular, we consider two additional columns on each side of the chessboard and impose squares lying there to remain always inactive. On the upper and lower part, as we mentioned above, we consider

https://doi.org/10.1017/S0956792520000418 Published online by Cambridge University Press

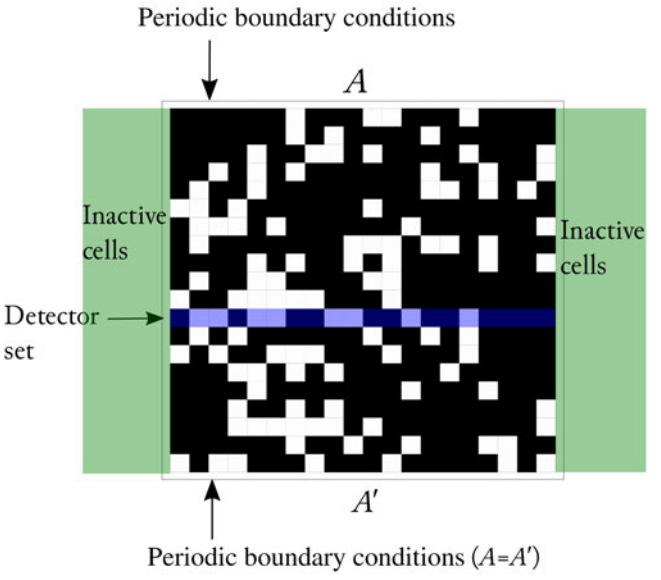

FIGURE 3. A typical initial configuration for $p = 0.3$, $N = 20$. Active (respectively inactive) cells are depicted in white (respectively in black). Boundary A is identified with boundary A'. Cells on green sides right and left are considered inactive. The detector set is identified with any given row; simulations yield similar results for any selected row due to the periodic boundary conditions imposed.

periodic boundary conditions taking rows $N + 1$ and $N + 2$ as identical copies of rows 1 and 2, respectively, for computational purposes.

(b) Any of the squares b_{ij}, which was initially active, remains in this state after one time step if the number of its active neighbours was equal either to 2 or 3, and it becomes inactive otherwise.

(c) After one time step, any of the squares b_{ij}, which was initially inactive, becomes active if it has three neighbours activated and remains inactive otherwise.

In order to study how activation and deactivation patterns proceed, we will follow the time series of values 1 (corresponding to an active state) and 0 (inactive state) as the simulation proceeds. In this way, for each of the squares, we will obtain a time series with values 0 and 1 as the system evolves. We will focus our attention on the time series corresponding to the squares touching on the generatrix line described above, which is fixed but otherwise arbitrary. Such line will be termed as a detector set. A typical initial configuration for $p = 0.3$ is shown in Figure 3. Keeping to the case $p = 0.3$ and following the rules described in a) to c) above, we perform 50 rounds (batches) of 100 time steps each. The final configuration obtained at the end of the first 100 time steps is then taken as the initial configuration for the next round, and such process is iterated 50 times. During the simulations, we keep track of the following parameters:

(d) The mean length of the consecutive time intervals in which the cell remained active.

(e) The mean length of the consecutive time intervals where the cell remained inactive.

(f) We finally compute the average of each simulation round for each cell in the detector set.

Simulations were performed using Julia programming language (see [3]).

https://doi.org/10.1017/S0956792520000418 Published online by Cambridge University Press

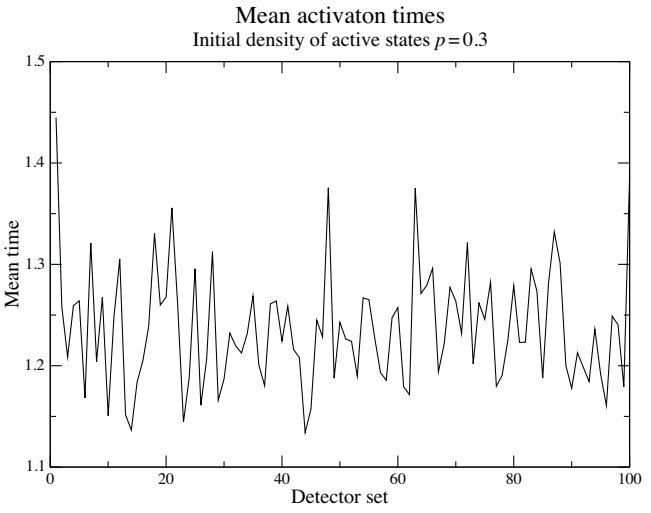

FIGURE 4. Mean activation time (the mean value of the lengths of intervals of continued activation) for an initial density of activated states $p = 0.3$.

For convenience of the reader, we will illustrate the previous rules for a simulation involving 10 time steps for one fixed square over an example. Let us denote by $h = (0, 0, 0, 1, 1, 0, 0, 0, 1, 0)$ the history of the active and inactive states. Then the lengths of the periods of active states are given by $a_{\text{lengths}} = (2, 1)$ whereas that of inactive states are given by $i_{\text{lengths}} = (3, 3, 1)$. The mean length of active states is therefore 1.5 and that of inactive states is 2.33. This is easily extended to the case where the number of time steps is taken to be 100 (or any other number for that matter) as in our simulations. In this way, two numbers are obtained for each square in the detector set. These are, respectively, termed as the mean activation and inactivation times. We then iterate the process 50 times and average the figures obtained for each square considered. The results thus obtained are shown in Figures 4 and 5.

From the previous figures, we notice that a clear recursive pattern of activation and inactivation is shown to unfold along the detector set. Moreover, the mean of activation and deactivation times display a considerable regularity along different square cells in the detector set. In particular, any square remains active for a mean time between 1.15 and 1.35 time steps and remains inactive between 5.5 and 8.5 time steps.

We next compare the results obtained from different choices of the initial configurations and different values of the initial density p. To this end, we performed the same simulations as before but starting from 100 random initial states for each fixed value of p and allowed then p to vary between 0.1 and 0.5. We then gathered the results for fixed p and took the mean for each cell in the detector set. Interestingly, mean activation time regularity is maintained when p lies in the range described above. The results obtained are gathered in Figure 6.

Figure 6 shows that there is a remarkable regularity in the activation patterns along the detector set, except for the results on the left and right extremes which represent artefacts associated with the artificial boundary conditions selected in a) above and which, as observed before, do not affect the actual bone domain. In Figure 7, we show the corresponding results for inactive states. Remarkably, as the initial density p of active states approaches 0.5, a striking phenomenon is observed. Namely, the mean inactivation times sharply increase as p tends to 0.5.

https://doi.org/10.1017/S0956792520000418 Published online by Cambridge University Press

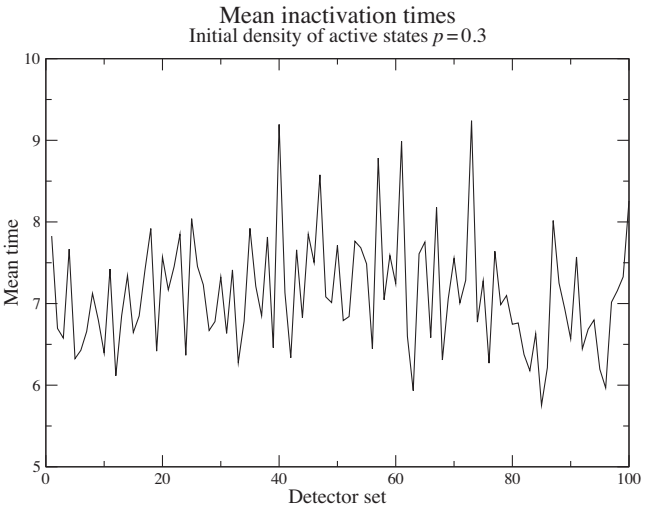

FIGURE 5. Mean inactivation times along the detector set for the situation considered in Figure 4.

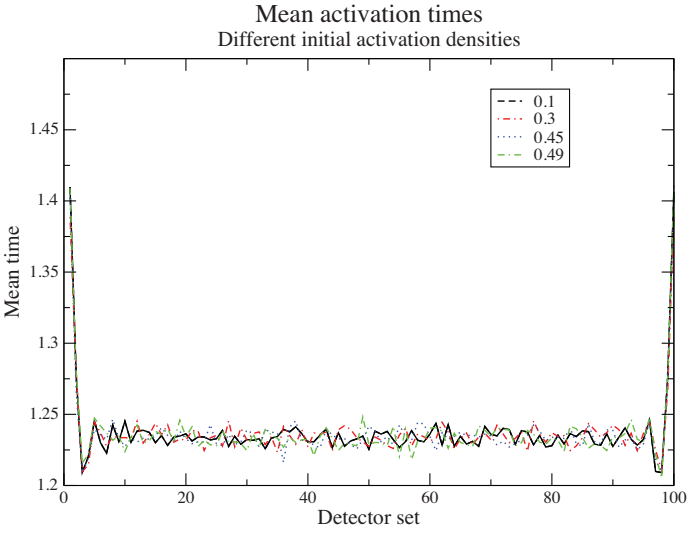

FIGURE 6. Activation patterns along the detector set for different values of the initial activation density p.

As Figures 6 and 7 show, the irregularity in the distribution of the mean activation and deactivation times (measured for instance by the variance of the corresponding distributions) is much lower than in Figures 4 and 5. This is a consequence of the fact that we are now taking mean values over several initial conditions for each value of p. The mean activation time then remains between 1.20 and 1.25 steps, while the mean inactivation time is close to 7 time steps for probabilities in $[0.1, 0.3]$ but grows unbounded as the probability of initially active states approaches 0.5.

https://doi.org/10.1017/S0956792520000418 Published online by Cambridge University Press

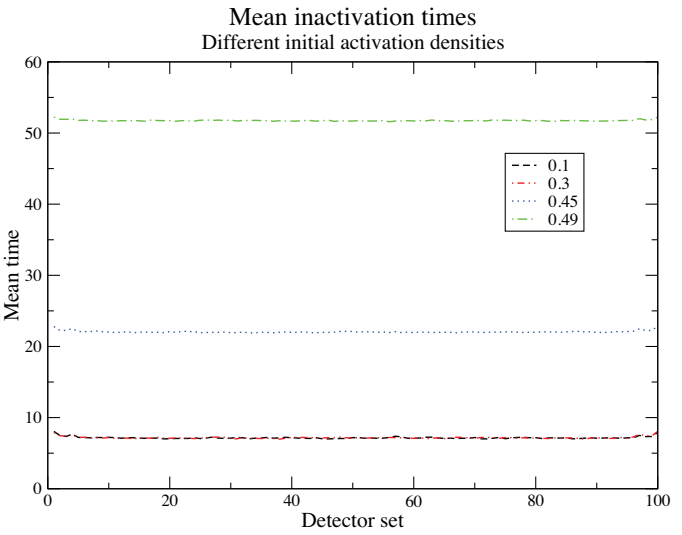

FIGURE 7. Inactivation patterns along the detector set for different values of the initial activation density p. Note the significant increase observed as p approaches 0.5 from below.

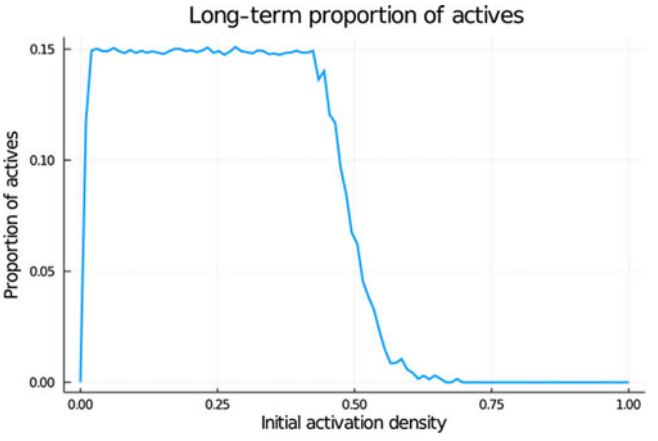

FIGURE 8. Evolution of the proportion of active cells in terms of its initial distribution p. Note the significant role played by the value $p = 0.5$. The proportion of active cells is computed after 500 time steps, and the result being plotted is computed for 100 different initial distributions and then averaged out. Computations were made for 100 different values of p, equally distributed between $p = 0$ and $p = 1$.

We next remark on the long-term behaviour of the model considered. To begin with, we point out that if the initial proportion of active cells is large enough (i.e., if $p > 0.5$), a dramatic drop in the proportion of active cells eventually occurs and most of the domain becomes inactive. On the other hand, if we start from a distribution where the proportion of active cells is quite small, no further depletion happens, and the proportion of active cells eventually settles around a positive value which does not exceed that corresponding to $p = 0.15$; see Figure 8. A close-up of the plot corresponding for initial distributions of active cells $p < 0.05$ is then provided in Figure 9.

https://doi.org/10.1017/S0956792520000418 Published online by Cambridge University Press

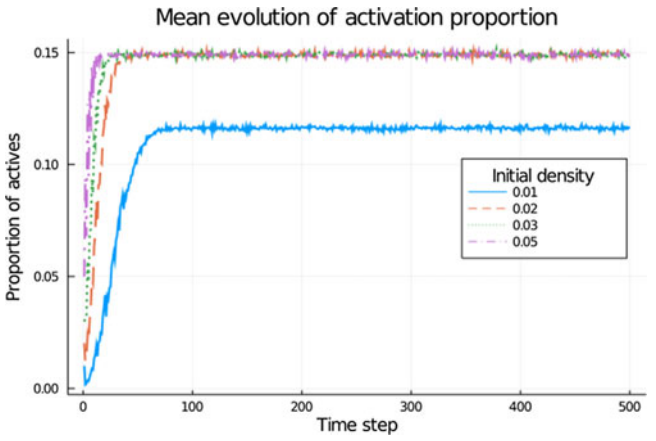

FIGURE 9. Mean evolution of activation proportion when the initial distribution of active cells lies in the range $0 < p < 0.05$. Note the (local) attractor character of the value $p = 0.15$. Large-time behaviour for data corresponding to very small proportions (say $p = 0.01$, depicted in blue) can be identified, if computations are allowed to run for longer time intervals. For instance, the case corresponding to the value $p = 0.01$ (depicted in blue) eventually converges to the pattern corresponding to $p = 0.12$.

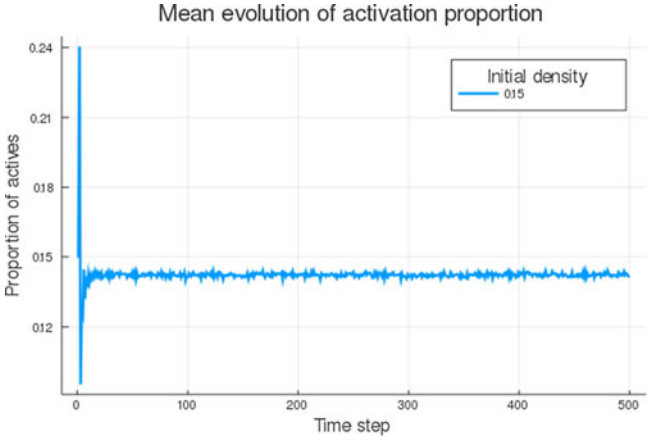

FIGURE 10. Mean evolution of the activation proportion starting from an initial value $p = 0.15$ after performing artificial inactivation of an internal 20×20 cells square. The system largely recovers and settles around a lower value $p = 0.12$. Deletion of smaller regions results in a lower impact on the asymptotic trend of the system, whereas imposing larger inactivation may lead to virtual blackout (data not shown).

We conclude this section with a remark on the resilience of the proposed mechanism under external perturbations, an issue which might be relevant when discussing the precise manner in which a homoeostatic screening process should be connected with the onset of bone remodelling. To this end, we considered the particularly relevant case of the initial distribution $p = 0.15$. We started from an arbitrary initial distribution and then imposed that an internal square of 20×20 cells should remain inactive henceforth. Simulations shown in Figure 10 show that, after a short initial transient, the mean evolution of the proportion of active cells settles around a stable value $p = 0.12$, a bit lower than the initial one.

https://doi.org/10.1017/S0956792520000418 Published online by Cambridge University Press

3 Discussion

Bone remodelling is a fascinating, exquisitely regulated homoeostatic mechanisms that allows the human skeleton to carry out its crucial functions during a lifetime, in spite of the continuous challenges that such organ has to sustain. As in any successful engineering structure, keys to an efficient operational activity rely not only in the excellence of its design but also on that of its maintenance systems. It is known that any single piece of bone is marked for renewal several times during a person's life. Once such renewal has been decided, dedicated teams of specialised cell types called Bone Multicellular Units (BMUs) are set in place to carry out such activity. Remarkably, the gathering and subsequent disbanding of BMUs once their task has been done seem to take place in the absence of any central coordinating system. In other words, decisions are locally made and locally executed. Moreover, such activity is simultaneously carried out in many different places along the skeleton at any given time.

In this work, we propose that, previous to any actual remodelling action, a thorough screening process is continuously at work over the whole skeleton, and it is only after this exploration mechanism has targeted a particular region for remodelling that BMUs are called in place to start their job. When searching for bone cells to be involved in that quality control process, osteocytes, the most frequent bone cell type, are main candidates. In spite of the fact that they are unable to move, they provide an extensive network of sensors that is able to exchange information among themselves, much as a neural network can do. Moreover, among the various chemical cues osteocytes are known to produce (and to react to), there is one in particular, sclerostin, which has been shown to be instrumental in the regulation of the BMU machinery [8, 22]. Roughly speaking, sufficiently high levels of sclerostin inhibit the recruiting of osteoblast and osteoclast precursors needed to provide bone demolition and its posterior reconstruction. However, when sclerostin levels are low enough, the road is open for remodelling to start. Bearing these facts in mind, an attempt has been made in this work to provide a minimal algorithm that could display thorough screening properties while involving only a regular network of sensors, any of which can flip among two different states, that we have called for convenience active and inactive, respectively. According to the biological background, we are keeping track of, in the first approximation, such states might respectively correspond to high and low levels of sclerostin expressed in the vicinity of each sensor. We then postulate transition rules between such states based in the celebrated Game of Life Cellular Automaton [10]. Starting with a simple set of rules, our simulations reveal striking hints about the way in which an actual screening mechanism might operate. In particular, we have concerned ourselves here with a very simple geometrical setting and have considered a plane domain subdivided into an array of regularly spaced square cells. In the underlying biological model, such plane domain corresponds to, say, the lateral surface of a cylindrical bone piece as that represented in Figure 2. In such domain, a regular grid of square cells is assumed, each having in its centre an osteocyte, interconnected with its neighbours by a system of channels that has been mentioned before. We have shown here that if we start from any arbitrary initial distribution with a comparatively small percentage of active versus inactive osteocytes (specifically, when the initial density of active cells p lies below 0.5), the transition rules proposed give raise to a moving, recurrent activation pattern. More precisely, if we focus our attention in one particular row in the geometric domain, we see that any square touching this line (and by extension, the osteocyte lying inside) will eventually, and recurrently, change its state. This means that if it was inactive at the initial time, it will change to an active state after some time steps, to eventually return to its former state afterwards. The algorithm allows this switching to be

https://doi.org/10.1017/S0956792520000418 Published online by Cambridge University Press

repeated indefinitely. The results obtained are discussed with regard to their dependence on the initial ratio p between active and inactive states when p ranges from $p = 0.1$ to $p = 0.5$. For such values of p, we observe the recurrence phenomenon previously described: every single cell in any selected row (that we have termed a detector set) is eventually changed from its initial state and eventually returns to it. Interestingly, the time interval (measured in terms of the algorithm time steps) when a detector cell remains active (that is, ready for remodelling) is substantially lower than the time spent in an inactive state (see Figures 4 and 5). As a matter of fact, the time any cell in the detector set is activated remains basically the same as p increases (see Figure 6), but the time it remains inhibited dramatically increases as p approaches $p = 0.5$, as shown in Figure 7. We have also studied the evolution of the proportion of active cells in terms of the corresponding initial distribution p. The results described in Figures 8 and 9 suggest a relevant role for the particular value $p = 0.15$, since this is the proportion around which initial distributions arising from a wide range of values $p < 0.5$ eventually stabilise. When p goes beyond the threshold value $p = 0.5$, a sudden drop occurs, and global inactivity will be imposed over a large part of the domain. This is shown in Figure 8. Figure 9 provides a close-up to the evolution arising from small initial values of p, the region where initial values $p > 0.5$ quickly fall into. It is shown in that figure that initial values above $p = 0.02$ eventually converge to the dominant pattern $p = 0.15$. Below that former value, however, other possible limits for the asymptotic distribution appear; for instance, $p = 0.01$ eventually settles into $p = 0.12$. We have concluded our study with a short discussion on the effect of imposed inactivation in a part of the considered domain, a situation which is reminiscent of the appearance of a microfracture in a bone piece. We noticed a substantial algorithmic resilience against such external perturbations. In particular, as noticed in Figure 10, we observed that starting from the particularly relevant value $p = 0.15$, inactivation of a relatively large interior square (20×20 cells) does not completely disrupts the screening algorithm, although it switches it towards a slightly lower mean value of activation $p = 0.12$. Taking out smaller or larger regions lead to proportional disruption results, as can be expected.

Summing up, the algorithm proposed in this work provides a simple, and robust, mechanism that ensures thorough screening in an appropriate timescale for any given planar domain. In our view, this makes this algorithm a reasonable candidate to be considered as a precursor in any biologically inspired model for bone remodelling. However, a number of questions have to be ascertained before this, or any related model, can be tested against biological data. To begin with, and at a mathematical level, the case of more involved 3D domains should be explored. In addition to this requirement, that we consider technically feasible, more serious, biologically minded challenges need to be addressed. To mention but one of these, ascertaining the algorithmic interface between the screening mechanisms and the onset of locally distributed BMUs requires deeper understanding of the biology involved. We can only hope that this initial step could be of some help to pursue such a goal.

Acknowledgements

CFA, MAH and GEO have been partially supported by MINECO Grant MTM2017-85020-P. JML was partially supported by grants PI18/01757 from Instituto de Salud Carlos III (Madrid, Spain). FB is grateful to the Roechling Foundation for its support.

Conflict of interest

Clemente Fernández Arias, Federica Bertocchini, Miguel Ángel Herrero, José Manuel López and Gerardo Oleaga declare that they have no conflict of interest.

References

[1] Office of the Surgeon General (US). Bone health and osteoporosis: A report of the surgeon general. Rockville (MD): Office of the Surgeon General (US); 2004. Available from: https://www.ncbi.nlm.nih.gov/books/NBK45513/

[2] Arias, C. F., Herrero, M. A., Echeverri, L. F., Oleaga, G. E., & López, J. M. (2018). Bone remodeling: A tissue-level process emerging from cell-level molecular algorithms. PloS One, **13**(9), e0204171.

[3] Bezanson, J., Edelman, A., Karpinski, S. & Shah, V. B. (2017) Julia: A fresh approach to numerical computing. *SIAM Rev.* **59**(1), 65–98.

[4] Crockett, J. C., Rogers, M. J., Coxon, F. P., Hocking, L. J. & Helfrich, M. H. (2011) Bone remodelling at a glance. *J. Cell Sci.* **124**, 991–998.

[5] Dallas, S. L., Prideaux, M. & Bonewald, L. F. (2013) The osteocyte: An endocrine cell . . . and more. *Endocr. Rev.* **34**(5), 658–690.

[6] Deutsch, A. & Dormann, S. (2017) *Cellular Automaton Modeling of Biological Pattern Formation*, Birkhäuser Ed. Basel.

[7] Echeverri, L. F., Herrero, M. A., López, J. M. & Oleaga, G. E. (2015) Early stages of bone fracture healing: Formation of a fibrin collagen scaffold in the fracture hematoma. *Bull. Math. Biol.* **77**, 156–183.

[8] Eriksen, E. F. (2010) Cellular mechanisms of bone remodeling. *Rev. Endocr. Metab. Disord.* **4**(11), 219–227.

[9] García-Aznar, J. M., Rueberg, T. & Doblaré, M. (2005) A bone remodelling model coupling microdamage growth and repair by 3d BMU activity. *Biomech. Model Mechanobiol.* **4**, 147–167.

[10] Gardner, M. (1970) Mathematical games - the fantastic combinations of John Conway's new solitary game life. *Sci. Am.* **223**, 120–123.

[11] George, D., Allena, R. & Remond, Y. (2018) A multiphysics stimulus for continuum mechanics bone remodelling. *Math. Mech. Complex Syst.* **6**(4), 307–319.

[12] Giorgio, I., dell'Isola, F., Andreaus, U., Alzahrani, F., Hayat, T. & Lekszycki, T. (2019) On mechanically driven biological stimulus for bone remodelling as a diffusive phenomenon. *Biomech. Model. Mechanobiol.* **18**(6), 1617–1663.

[13] Graham, J. M., Ayati, B. P., Holstein, S. A. & Martin, J. A. (2013) The role of osteocytes in targeted bone remodeling: A mathematical model. *PLoS One* **8**(5), e63884.

[14] Hadkidakis, D. J. & Androulakis, I. I. (2006) Bone remodeling. *Ann. N. Y. Acad. Sci.* **1092**(1), 385–396.

[15] Hattner, R., Epker, B. N. & Frost, H. M. (1965) Suggested sequential mode of control of changes in cell behaviour in adult bone remodelling. *Nature* **206**(4983), 489–490.

[16] Husain, A. & Jeffries, M. A. (2017) Epigenetics and bone remodeling. *Curr. Osteoporos Rep.* **15**(5), 450–458.

[17] Kenkre, J. S. & Basset, J. H. D. (2018) The bone remodeling cycle. *Ann. Clin. Biochem.* **55**(3), 308–327.

[18] Köhn-Luque, A., de Back, W., Starruss, J., Mattiotti, A., Deutsch, A., Pérez-Pomares, J. M. & Herrero, M. A. (2011) Early embryonic vascular patterning by matrix-mediated paracrine signalling: A mathematical model study. *PLoS ONE* **6**(9), e24175.

[19] Komarova, S. V., Smith, R. J., Dixon, S. J., Sims, S. M. & Wahl, L. M. (2003) Mathematical model predicts a critical role for osteoclast autocrine regulation in the control of bone remodeling. *Bone* **33**(2), 206–15.

[20] MacArthur, B. D., Please, C. P., Taylor, M. & Oreffo, R. O. C. (2004) Mathematical modelling of skeletal repair. *Biochem. Biophys. Res. Commun.* **313**, 825–833.
[21] Martínez-Reina, J., Reina, I., Domínguez, J. & García-Aznar, J. M. (2014) A bone remodelling model including the effect of damage on the steering of BMUs. *J. Mech. Behav. Biomed. Math.* **32**, 99–112.
[22] Noble, B. S. (2008) The osteocyte lineage. *Arch. Biochem. Biophys.* **473**, 106–111.
[23] Parfitt, A. M. (2002) Targeted and nontargeted bone remodeling: relationship to basic multicellular unit origination and progression. *Bone* **30**, 5–7.
[24] Park-Min, K. H. (2018) Mechanisms involved in normal and pathological osteoclastogenesis. *Cell Mol. Life Sci.* **75**(14), 2519–2528.
[25] Prisby, R. D. (2017) Mechanical, hormonal and metabolic influences on blood vessels, blood flow and bone. *J. Endocrinol.* **235**(3), R77–R100.
[26] Robling, A., Castillo, A. & Turner, C. (2006) Biomechanical and molecular regulation of bone remodeling. *Ann. Rev. Biomed. Eng.* **8**, 455–98.
[27] Ross, D. S., Mehta, K. & Cabal, A. (2017) Mathematical model of bone remodeling captures the antiresorptive and anabolic actions of various therapies. *Bull. Math. Biol.* **79**, 117–142.
[28] Rucci, N. (2008) Molecular biology of bone remodelling. *Clin. Cases Miner Bone Metab.* **5**(1), 49–56.
[29] Ryser, M. D., Komarova, S. V. & Nigam, N. (2010) The cellular dynamics of bone remodeling: A mathematical model. *SIAM J. Appl. Math.* **70**(6), 1899–1921.
[30] Siddiqui, J. A. & Partridge, N. C. (2016) Physiological bone remodeling: Systemic regulation and growth factor involvement. *Physiology (Bethesda)* **31**(3), 233–245.
[31] Sims, N. A. & Martin, T. J. (2014) Coupling the activities of bone formation and resorption: A multitude of signals within the basic multicellular unit. *BoneKEy Rep.* **3**, 481.
[32] Zaidi, M. (2007) Skeletal remodeling in health and disease. *Nat. Med.* **13**, 791–801.

https://doi.org/10.1017/S0956792520000418 Published online by Cambridge University Press